Fine-Resolution Mapping of Fine Dust Concentration in Urban Areas and Population Exposure Analysis via Dispersion Modeling

Seungwoo Son [1], Dongwoo Kim [1], Youngeun Kang [2], Hyungjin Jeon [1,*],

Seogcheol Kim [3], Kyunghak Cho [3] and Jaejin Yu [1,*]

[1] Department of Land and Water Environment Research, Korea Environment Institute, Sejong 30147, Korea; swson@kei.re.kr (S.S.); dwkim@kei.re.kr (D.K.)

[2] Research Department, Site Planning Co., Ltd, Busan 48505, Korea; jiyoon8936@gmail.com

[3] Boolt Simulation, Inc, Seoul 06664, Korea; sckim@boolt.co.kr (S.K.); kyunghak@boolt.co.kr (K.C.)

*   Correspondence: hjjeon@kei.re.kr (H.J.); jjyu@kei.re.kr (J.Y.)

Abstract: It is currently difficult to obtain accurate fine dust information in residential areas due to the insufficient number of air quality monitoring systems and spatial imbalances. Therefore, a detailed particulate matter dispersion model including factors such as land use and meteorological information was developed in this study and used to create fine dust concentration distribution maps. The fine dust concentration distribution maps currently available to citizens were compared with those obtained by dispersion modeling, and population distribution data were employed to compare the populations exposed to fine dust according to the two methods. The results of the existing method and the developed particulate matter dispersion model differed significantly. For instance, the PM2.5 concentrations in Daejeon, South Korea, on February 17, 2018, were 56% "Good" and 44% "Moderate," according to the existing method, while they were 31% "Good," 26% "Moderate," 28% "Unhealthy," and 15% "Very Unhealthy," according to the dispersion model. Furthermore, the existing method indicated that no portion of the population was exposed to poor fine dust concentrations, while the proposed model revealed that over 170 thousand people were exposed to such concentrations. These results on fine dust distributions will contribute to sustainable urban and environmental planning.

Keywords: atmospheric pollution; dispersion modeling; particulate matter; urban and environmental planning, public health

1. Introduction

Atmospheric pollution is a major environmental issue that has critical impacts on society, the economy, and human health [1–3]. It is also regarded as one of the most significant environmental concerns of both the public and scientists for past few decades [4], related studies evaluating or monitoring its status, risk, and quality have been conducted worldwide [5-9]. Especially in urban areas, various atmospheric pollutants are generated in increasing amounts due to various types of land use and human activity. The severity of atmospheric pollutants is also growing in South Korea due to the development and revitalization of urban areas, and public interest in this matter is rising based on the increasing examples of the impacts of atmospheric pollution on health.

South Korea is particularly affected by its neighboring countries depending on the season, and the amount of fine dust is intensifying daily as a result of the traffic volume and industrial facilities in the cities. In accordance with such societal trends, the South Korean government provides information on fine dust to its citizens based on data collected from 323 Air Quality Monitoring Systems (AQMS) installed across the country. Fine dust is designated as PM10 and PM2.5, and the data about these particulates are provided in real time to citizens through a website and smartphone app. The AQMS, however, have significant installation and maintenance costs, and a lack of manpower for maintenance has resulted in a spatial imbalance in their installation. These devices are installed only in certain regions, and insufficiencies in the number of units make fine dust information monitoring difficult in wider regions. Determining the quantities and spatial distributions of fine dust

47 is of the utmost importance for environmental improvement in urban areas and long-term policy
48 implementation, but the delivery of accurate fine dust information to citizens is difficult due to the
49 aforementioned issues. Research is being conducted on prediction of past spatial distributions of fine
50 dust in order to resolve these issues.
51   Traditional methods of predicting spatial distributions of air quality, such as the amount of fine
52 dust, include using the closest measurement data or the average values for an entire region [10, 11].
53 If one searches for air quality information about a certain place in Korea, the measurements from the
54 closest AQMS are queried. However, high-resolution atmospheric pollutant distribution information
55 is necessary to establish policies on urban planning, the environment, and health [12]. Various
56 interpolation techniques such as kriging and inverse distance weighting (IDW) are being developed
57 and utilized as spatial statistics methods to estimate values in locations that have not been measured.
58 These methods are based on singular variables, but the distributions of atmospheric pollutants should
59 be predicted using assorted variables according to the circumstances of the target areas because air
60 quality is affected by complex processes, including climate, temperature, terrain, pollution source
61 location, traffic volume, and land use [13].
62   Recently, studies have been conducted in which artificial intelligence (AI)-based artificial neural
63 networks (ANNs) and machine learning were utilized by applying numerous variables to increase
64 the prediction accuracy. Studies have also been conducted on Beijing, China, in which the universal
65 kriging technique was employed to obtain fine dust distribution maps based on climate data and data
66 collected by fine dust sensors [14]. In addition, atmospheric pollutant distribution prediction has been
67 investigated by utilizing ANNs, land-use regression models, and machine learning techniques that
68 account for factors that affect air quality distributions, such as those of fine dust [15–17].
69   The research methodologies for determining accurate air quality distributions are continually
70 being elaborated upon because they are utilized not only for spatial decision-making, but also by
71 individuals to make decisions regarding outdoor activities, which is especially critical for vulnerable
72 groups, such as children and the elderly. There are also many people who want to have accurate fine
73 dust information to make informed choices regarding outside activities or airing out their homes.
74 With the continually increasing interest in fine dust, spatial analysis of the population that is exposed
75 to fine dust is important.
76   An accurate survey of the population spread is first necessary to analyze the population that is
77 exposed to fine dust. Population estimates are conducted using methods such as Bayesian models
78 and random forests by downscaling population census data and analyzing the population spread [18,
79 19]. In these techniques, the population is calculated using a uniform spatial resolution of 100–1000
80 m units.
81   It is difficult to obtain accurate fine dust information for the residential districts of modern urban
82 areas due to the insufficient number of AQMS devices and their uneven spatial distribution.
83 Accordingly, the objective of the present study was to reduce the spatial imbalance of fine dust
84 information that is provided to citizens in order to minimize the public health risks from fine dust.
85 Specifically, land coverage, land use, emission source, and meteorological data were utilized to
86 develop a particulate matter dispersion model and to construct fine dust concentration distribution
87 maps. This article provides not only a comparison and analysis of the fine dust concentration
88 distribution information available to citizens, but also quantitative analysis of the population that is
89 exposed to fine dust based on elaborate population distribution data.

90 **2. Materials and Methods**

91   In the present study, Particulate matter dispersion modeling was utilized to examine the spatial
92 errors of the fine dust information that citizens currently receive. The overarching research
93 methodology employed was particulate matter dispersion modeling and geographic information
94 systems (GISs) to generate fine dust concentration maps and to analyze the exposed population. The
95 differences between the model developed in this research and the existing methodology were also
96 examined by comparing the fine dust concentrations and populations exposed to fine dust according
97 to the two methods. The overall methodology is illustrated in Figure 1.

98
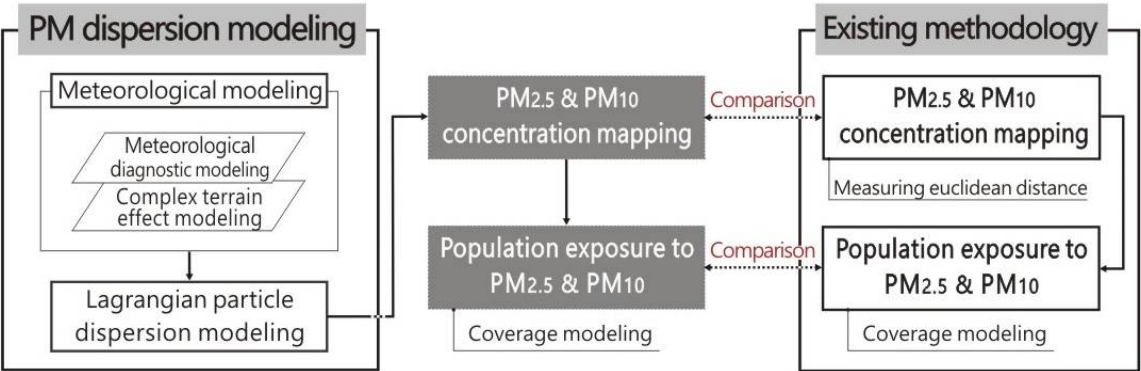
99
100
Figure 1. Diagram of overall research methodology.

101   *2.1 Study Site*

102   The study site was Daejeon Metropolitan City, which is located in the central region of South
103   Korea. Daejeon is a large city with a high population density. As one of the five largest metropolitan
104   cities in South Korea, Daejeon has an area of approximately 530 km², with a population of roughly
105   1.5 million people. Particulate matter dispersion modeling was conducted in a 6 km × 6 km area that
106   included the area surrounding the city hall where the population is concentrated (Figure 2).
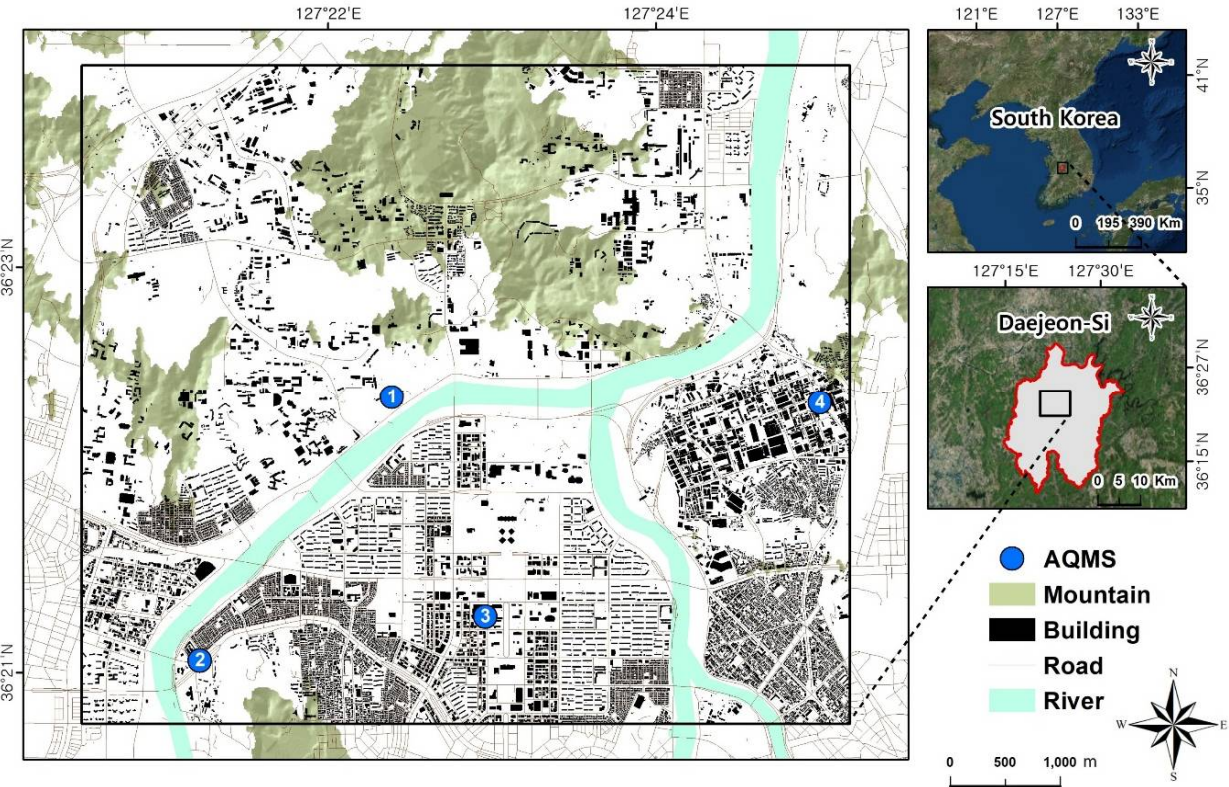
107
108
Figure 2. Study site.

109   The study site was divided into grids with a minimum size of 50 m, which includes the scale at
110   which the dispersion and movement of atmospheric pollutants in the city can be examined. Each grid
111   was analyzed to deduce its fine dust concentration.

112   *2.2 Particulate Matter Dispersion Modeling*

113   There are two main types of particulate matter dispersion models: meteorological models and
114   Lagrangian particle dispersion models. The overall particulate matter dispersion modeling process

115 used in this study is shown in Figure 3. The computer programming language Fortran 2003, which is
116 primarily utilized in scientific numerical analysis, was employed.
117
118

119
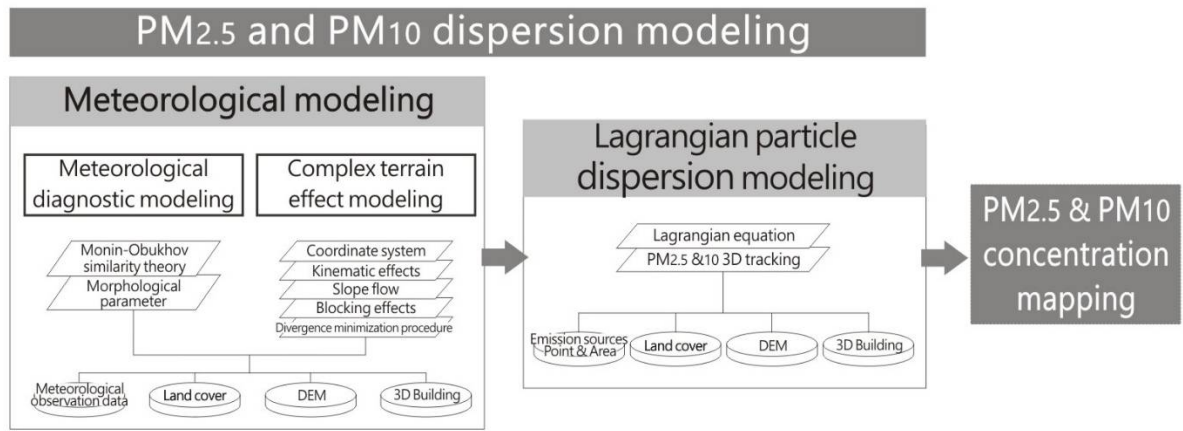
120 **Figure 3.** Particulate matter dispersion modeling process.

121   In meteorological modeling, meteorological observation dates, land coverage, digital elevation
122 models (DEMs), and 3D buildings are used as input data. Meanwhile, in Lagrangian particle
123 dispersion modeling, land coverage, DEMs, 3D buildings, and emission sources (points and areas)
124 are used as input data. These inputs are summarized in Table 1 below.

125 **Table 1.** Input data for particulate matter dispersion modeling.

Model		Input data	Description
Particulate matter dispersion modeling	Meteorological model	Meteorological observation data	Weather station information that is either included in the target site or can influence the target site
		Land coverage	Conversion of land coverage information about the target site into 50 m grid units
		DEM	Conversion of terrain information about the target site into 50 m grid units
		3D building	3D information about the buildings included in the target site
	Lagrangian particle dispersion model	Emission sources (point)	Hourly quantity of atmospheric pollutant emission from smokestacks of emitting industries (330 smokestacks)
		Emission sources (area)	Conversion of information regarding traffic volume and emission pollutants at the target site into road emission source information
		Land coverage	Conversion of land coverage information about the target site into 50 m grid units
		DEM	Conversion of terrain information about the target site into 50 m grid units
		3D building	3D information about the buildings included in the target site

126 2.2.1 Meteorological Modeling

127   In meteorological models, weather observations are used to generate detailed wind fields and

128　meteorological fields of target sites, and as diagnostic rather than prognostic models. Meteorological
129　models produce meteorological information that is identical to the weather observations at any point
130　in time [20].

131　　Because nearly 65% of South Korea is comprised of mountainous areas, terrain must be
132　considered, as there are also considerable terrain fluctuations in its cities. In addition, 3D
133　meteorological field modeling should be conducted that takes into account buildings and various
134　structures because South Korea has diverse infrastructure and a concentrated population. In
135　meteorological modeling, a primary meteorological field is generated that accounts for flat areas,
136　buildings, and structures through meteorological diagnostic modeling, and a final meteorological
137　field is generated by producing a secondary meteorological field through complex terrain modeling
138　that accounts for substantial terrain changes, such as those in mountainous regions.

139　　In atmospheric boundary layer modeling in flat regions, meteorological observations and
140　forecasts based on Monin–Obukhov similarity theory are utilized to generate meteorological
141　information about the atmospheric boundary layer. The vertical distribution ($u(z)$) of the average
142　wind velocity is given by Equation (1):

143　　$u(\text{z}) = \frac{u^*}{k}\left[\ln\left(\frac{z}{L}\right) - \Psi_m\left(\frac{z}{L}\right) + \Psi_m\left(\frac{z_0}{L}\right)\right].$　　　　　　　　　　　　(1)

144　Here, k is the von Kármán constant, u^* is the friction velocity, z is the vertical elevation calculated
145　from the surface, z_0 is the surface roughness, L is the Monin–Obukhov length, and Ψ_m is a
146　function that reflects atmospheric stability.

147　　The form of Ψ_m depends on L, and a functional formula presented previously was applied in
148　this study [20–22]. u^* and L are meteorological variables, but they must be calculated based on
149　meteorological observations because they are not physical quantities measured at weather
150　observation stations. L can be calculated using the following equation:

151　　$L = -\frac{pc_pT_{ref}u^{*^3}}{kgH}.$　　　　　　　　　　　　　　　　　　　　(2)

152　Here, p is the air density, c_p is the specific heat at constant pressure, T_{ref} is the observation
153　temperature, u^* is the friction velocity, k is the von Kármán constant, g is the gravitational acceleration
154　(9.8 m/s²), and H is the sensible heat flux.

155　　H was obtained by employing an empirical formula presented previously [20, 23]. As shown in
156　Equation (2), u^* and L are connected to one another, and because the value of just one of these
157　quantities cannot be calculated sequentially, an iterative scheme must be used to obtain the values of
158　both. In the iterative scheme described by Equation (1), Ψ_m is initially set to 0, and elevation and
159　wind speed observations are employed to calculate u^*. The obtained value of u^* is then used in
160　Equation (2) to calculate L, and hence to estimate Ψ_m. Next, the resulting value of Ψ_m is substituted
161　into Equation (1) to recalculate u^*, and the result is again substituted into Equation (2) to calculate L.
162　This process was repeated in this study for iterative calculation of u^* and L, and the deduced values
163　of u^* and L were compared. The calculations agreed to within the margin of error.

164　　Although urban areas are flat, their characteristically dense buildings and man-made structures
165　affect the air currents. Morphological parameters have been used to estimate airflow distributions
166　considering buildings and man-made structures [20, 24–27]. Urban spaces were divided into 100 m ×
167　100 m grid units to calculate the statistics of the building shapes for each unit, and spaces with heights
168　of 100 m from the ground were set as the morphological model domains.

169　　The primary meteorological field was generated through meteorological diagnostic modeling in
170　the target sites, where flat areas, buildings, and structures were accounted for through the above
171　processes.

172　　Complex terrain effect modeling was conducted to generate a secondary meteorological field.
173　Urban areas with significant mountainous terrain can be affected considerably by the terrain. The
174　terrain particularly affects the meteorological field adjacent to the ground surface. To account for the
175　complexities of the terrain in this study, the meteorological fields were calculated taking into account
176　five types of terrain effects, including coordinate system variations, kinematic effects, slope flow,

177 blocking effects, and divergence minimization procedures in the equation for deducing the
178 meteorological fields in flat areas.
179   For the grid system, the following equation was employed to generate a terrain-following
180 vertical coordinate system:

181    $X = x$, $Y = y$, $Z = z_p - h_T$.   (3)

182 Here, x and y are the horizontal coordinates, Z is the vertical coordinate, z_p is the rectangular
183 coordinate, and h_T is the altitude of the topography above sea level. In the vertical coordinate
184 system, the vertical wind speed (w) can be calculated by employing the following equation:

185    $w = w_p - u \frac{\partial h_T}{\partial x} - v \frac{\partial h_T}{\partial y}$.   (4)

186 Here, w_p is the vertical wind speed (m/s) in the vertical coordinate system, and u and v are the east–
187 west and north–south horizontal components (m/s) of the wind speed vector.
188   Kinematic effects reflect the tendency for airflow to form based on terrain, and w was calculated
189 using the following modified equation [28]:

190    $w = (\vec{V} \cdot \nabla h_T) \exp(-kz)$.   (5)

191 Here, $\vec{V}$ is the horizontal wind speed vector (u, v), and k is the vertical attenuation constant, which
192 changes based on the atmospheric stability.
193   The slope flow can be calculated using the following equation based on the airflow that occurs
194 due to differences in density along slopes [29]:

195    $S = S_e [1 - exp(-x/L_e)]^{1/2}$.   (6)

196 Here, S is the slope flow, S_e is the slope flow that reaches an equilibrium state, x is the distance
197 from a valley to a slope, and L_e is the length to the arrival of an equilibrium state. S_e and L_e can be
198 calculated by applying the following equations:

199    $s_e = [hg(\Delta\theta/\theta) \sin\alpha/(C_d + k)]^{1/2}$ (7)
200    $L_e = h/(C_D + k)$.   (8)

201 Here, h is the depth of the slope flow, g is the gravitational acceleration, $\Delta\theta$ is the potential
202 temperature loss that occurs due to surface cooling, α is the elevation angle of a horizontal slope, C_D
203 is the frictional force drag coefficient of the ground, and k is the model coefficient of the highest
204 point of a gradient current.
205   Blocking effects occur when the atmospheric layer is stratified in a stable form due to the surface
206 cooling effect, and airflow rotates on the peripherals rather than passing over the projecting terrain.
207 The effects of blocked flow in a given direction due to the terrain are reflected by the Froude number
208 [30], which can be calculated using the following equation:

209    $F_r = \frac{V}{N\Delta h_T}$.   (9)

210 Here, F_r is the local Froude number, V is the grid wind speed (m/s), N is the Brunt–Vis frequency
211 (1/s), and Δh_T is the effective height (m) of the protruding terrain.
212   Lastly, the divergence minimization procedure must be considered. The divergence of the wind
213 field where the terrain effect is reflected must be kept close to 0. The divergence at each grid point
214 can be calculated using Equation (10):

215    $D_{ijk} = \frac{w_{i,j,k+1/2} - w_{i,j,k-1/2}}{z_{k+1/2} - z_{k-1/2}} + \frac{u_{i+1,j,k} - u_{i-1,j,k}}{2\Delta x} + \frac{u_{i,j+1,k} - u_{i,j-1,k}}{2\Delta y}$.   (10)

216 Here, D_{ijk} is the divergence (1/s) of grid point (i, j, k), and Δx and Δy are the grid intervals (m) in
217 the x and y directions, respectively. The secondary meteorological field was generated through
218 complex terrain effect modeling in areas that account for complex terrain, such as mountainous
219 terrain, by employing the processes described above.
220   The primary and secondary meteorological fields were used to generate the final meteorological

221 field, as shown in Equation (11):

222 $u = \omega\, u_1 + (1 - \omega)u_2$

223 $v = \omega\, v_1 + (1 - \omega)v_2$

224 $w = \omega\, w_1 + (1 - \omega)w_2.$ (11)

225 Here u, v, and w are the east and west components, the north and south components, and the vertical
226 components of the wind respectively. u_1, v_1, and w_1 are the airflows of the primary meteorological
227 field considering flat terrain, buildings, and structures; u_2, v_2, and w_2 are the airflows of the
228 secondary meteorological field above complex terrain; and ω is a weight function variable established
229 based on the number and elevation of the weather observation station; it has a real value between 0
230 and 1. If the complex terrain effect is marginal, as in $u_1 \cong u_2$, $v_1 \cong v_2$, and $w_1 \cong w_2$, the first
231 meteorological field may be viewed as the final meteorological field.

232 2.2.2 Lagrangian Particle Dispersion Modeling

233   Lagrangian particle dispersion models are popular tools for simulating the dispersion of trace
234 gases, aerosols, or radionuclides in the atmosphere [31–35]. These models are primarily utilized as
235 atmospheric diffusion models and as sophisticated models for calculating changes in wind direction.
236 Due to topographic characteristics and chemical changes in pollutants based on time, they can trace
237 the migration of air masses [14]. In Lagrangian particle dispersion modeling, particle movements
238 during a time dt (s) can be expressed as Langevin equations [36]:

239 $$du = -\frac{u}{T_{Lu}}dt + \sqrt{C_0 \epsilon dt}\,\omega_u$$

240 $dv = -\dfrac{v}{T_{Lv}}dt + \sqrt{C_0 \epsilon dt}\,\omega_v$

241 $dw = -\dfrac{w}{T_{Lw}}dt + \sqrt{C_0 \epsilon dt}\,\omega_w.$ (12)

242 Here, T_{Lu}, T_{Lv}, and T_{Lw} are the Langrangian time scales of the x, y, and z directions, respectively,
243 which can be defined as in Equation (13):

244 $T_{Lu} = 2\dfrac{\sigma^2{}_u}{C_0 \epsilon}$

245 $T_{Lv} = 2\dfrac{\sigma^2{}_v}{C_0 \epsilon}$

246 $T_{Lw} = 2\dfrac{\sigma^2{}_w}{C_0 \epsilon}.$ (13)

247 Here, $\sigma^2{}_u$, $\sigma^2{}_v$, and $\sigma^2{}_w$ are the turbulent energies (m²/s²) in the x, y, and z directions, respectively.

248 2.2.3 Particulate Matter Dispersion Modeling Verification and Mapping

249   To verify the modeling, the work conducted by [37], which is widely quoted in literature related
250 to atmospheric diffusion in the field of fluid dynamics, was employed in this study. [37] designed a
251 sophisticated wind tunnel experiment and performed a thermal diffusion experiment. In the present
252 study, the variables and environment used in the wind tunnel experiment were implemented, and
253 the particulate matter dispersion modeling was verified by comparing the data obtained in this study
254 with those of [37].
255   The movement and dispersion of fine dust change continually based on the wind direction, wind
256 speed, weather conditions, and natural or artificial environments. Thus, fine dust concentrations can
257 be visualized in 1 h intervals based on weather observations. The PM2.5 and PM10 concentration
258 standards are divided by each of their concentrations. The concentration of PM2.5 is designated as
259 "Good" when it is 0–15 µg/m³, "Moderate" when it is 16–35 µg/m³, "Unhealthy" when it is 36–75
260 µg/m³, and "Very Unhealthy" when it is over 76 µg/m³, while that of PM10 is designated as "Good"

261   when it is 0–30 µg/m³, "Moderate" when it is 31–80 µg/m³, "Unhealthy" when it is 81–150 µg/m³, and
262   "Very Unhealthy" when it is over 151 µg/m³. These are the fine dust concentration standards
263   currently provided to citizens and are similar to those advised by developed nations and the World
264   Health Organization (WHO).

265   *2.3 Comparison with Existing Methodology and Analysis*

266   2.3.1 Comparison and Analysis of Fine Dust Concentration Maps

267   As mentioned previously, the fine dust concentrations that are currently provided to citizens by
268   the state provide concentrations measured in real time at AQMS in 1 h intervals. Queries for
269   concentrations can be done via the internet or a smartphone to obtain the concentrations from the
270   AQMS closest to the current location of the user. The closest fine dust concentrations can be
271   determined using the Euclidean distance measurement method. In this study, the fine dust
272   concentration maps deduced through Euclidean distance measurement were compared with those
273   deduced using the particulate matter dispersion model developed in this study, and the differences
274   were analyzed. GIS ArcMap 10.3 was used for the Euclidean distance measurements.

275   2.3.2 Comparison and Analysis of Population Exposed to Fine Dust

276   The exposed population was calculated, compared, and analyzed based on fine dust maps
277   constructed using the existing methodology and particulate matter dispersion modeling. Census data
278   were employed to determine the exposed population. The census data included the population
279   residing in buildings and were provided by the state as populations within 100 m × 100 m areas.
280   Downscaling these data, the population was calculated within 50 m × 50 m units for the target site in
281   this study. A coverage model [32, 33] was employed for the population calculations within the
282   concentration map, using the following equation:

283    $\text{Coverage} = \sum_p S_p.$ (14)

284   Here, S_p is the distribution area by fine dust concentration, and p is the population.

285   **3. Results**

286   *3.1 Particulate Matter Dispersion Modeling Verification and Mapping*

287   In the simulations conducted in the present research, the variables were implemented to model
288   an environment such as that used by [37], and the results of their wind tunnel experiment were
289   compared with those obtained using the model developed in this study. Figure 4(a) depicts the data
290   from the wind tunnel experiment conducted by [37], which are overlapped with the results of this
291   study in Figure 4(b).

292
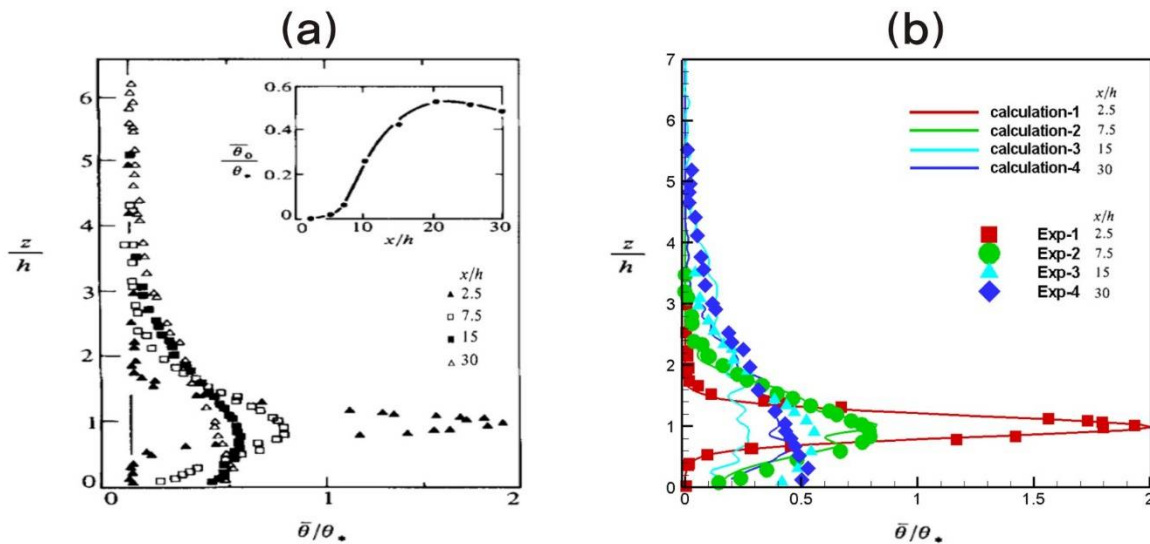
293   **Figure 4.** (a) Data from the wind tunnel experiment conducted by Raupach and Legg [37], and (b) overlapping
294   of the data from this study with that obtained by Raupach and Legg [37]. x/h is the distance from the source
295   point, h is the height of the source emissions, $\overline{\theta_0}$ is the air temperature relative to the ambient air
296   temperature, and θ_* is the temperature scale. The calculations of Raupach and Legg [37] are designated as
297   "Exp," and those obtained using the model developed in this study are designated as "calculation."

298   The experimental results obtained in four environments (a–d) were compared based on the
299   distance from the source point, and R^2 was used to analyze the relationships between the data
300   obtained in this study and those of [37] (Figure 5).
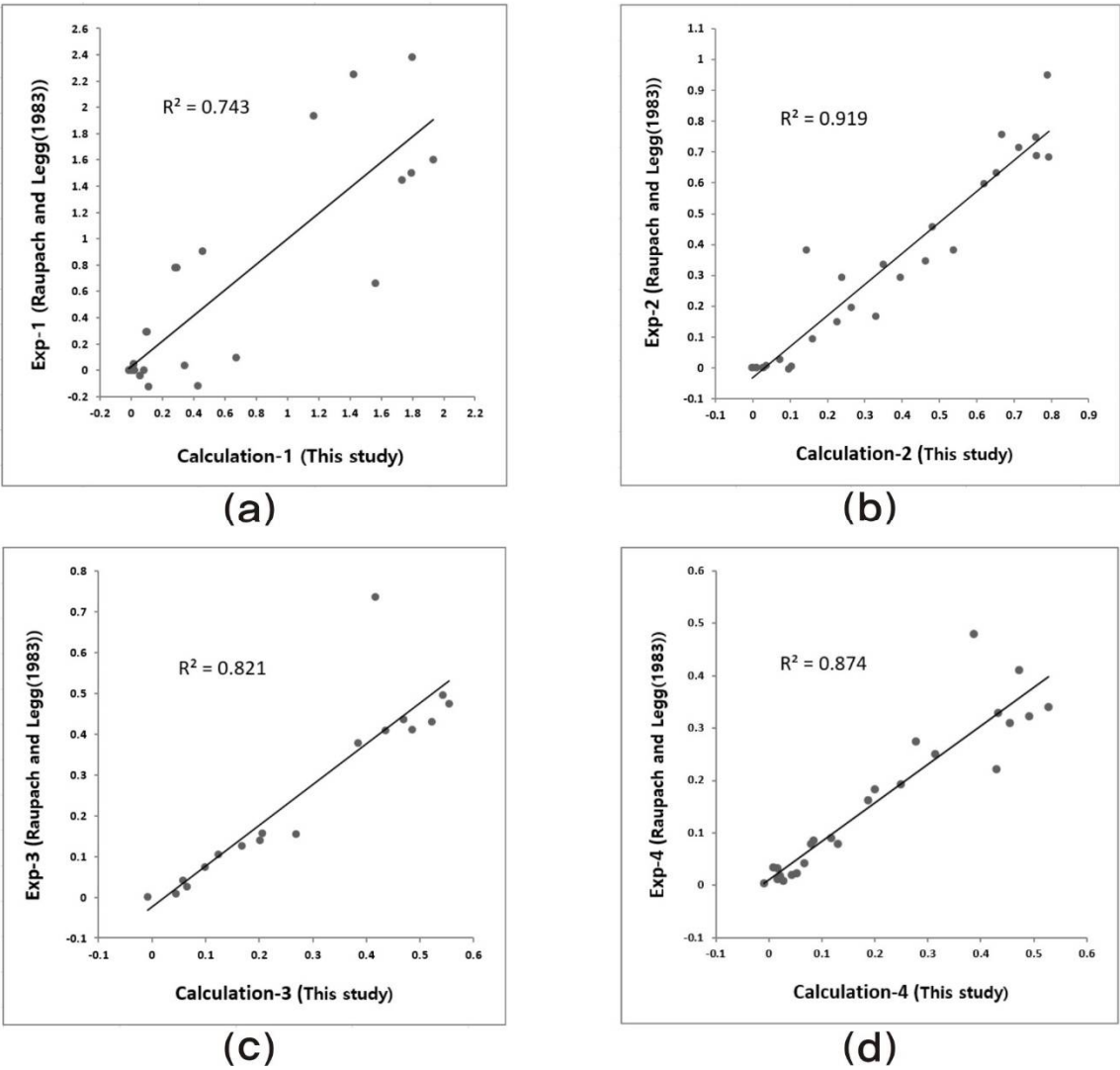
Figure 4. Correlation analysis of the results obtained in the preceding research with those of the present study. (a)–(d) Comparison of the experimental results obtained in four environments based on distance from the source point.

The R^2 values in environments (b) demonstrates exceptionally high explanatory power above 0.9. Environments (a), (c) and (d) also exhibit high explanatory powers, above 0.7 and 0.8, respectively, demonstrating that the model developed in this study provides results similar to those obtained in the preceding research.

Fine dust concentration maps based on input data from 1 h intervals can be constructed in 1 h intervals in particulate matter dispersion modeling. In this study, concentration maps were created based on a large amount of fine dust data, and the relationships between the results from particulate matter dispersion modeling and the data from AQMS was observed. Figure 6 depicts the PM2.5 concentration maps obtained via dispersion modeling in the areas surrounding AQMS units.

314
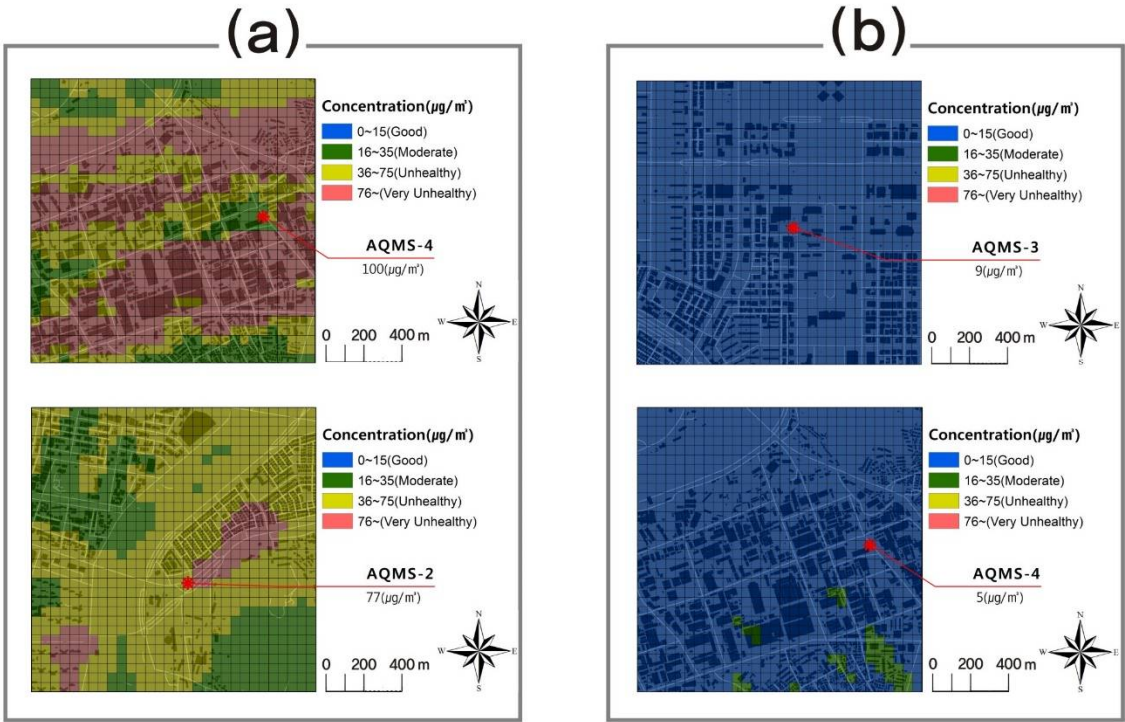
Figure 5. PM2.5 dispersion modeling results. Days with (a) poor and (b) favorable amounts of fine dust according to the AQMS values.

Figures 6(a) and (b) present the PM2.5 dispersion modeling concentration maps for one day. Figure 6(a) shows that the fine dust concentration is generally poor, while Figure 6(b) shows that the fine dust concentration is generally good. Similar concentrations can be found by comparing the measured concentrations of AQMS.

Figure 7 presents the PM10 dispersion modeling results obtained in expanded areas surrounding the AQMS.

323
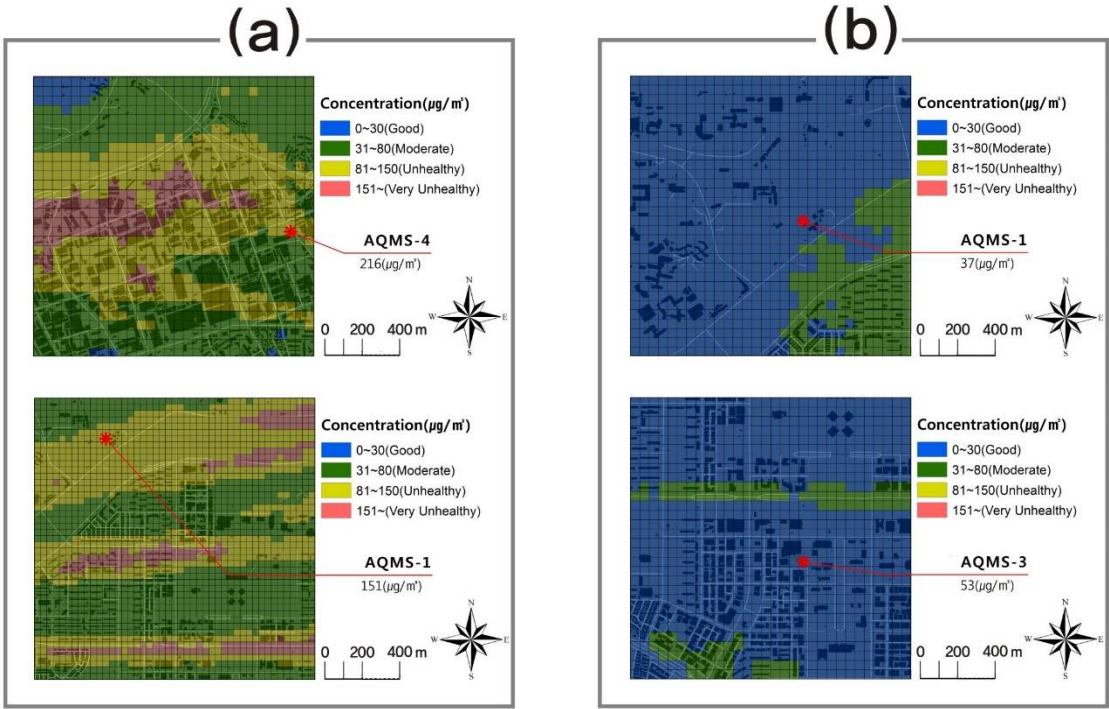
324 **Figure 6.** PM10 dispersion modeling results. (a) Days with poor fine dust values and (b) days with favorable
325 fine dust values in the AQMS values.

326   Figures 7(a) and (b) present the PM10 dispersion modeling concentration maps for one day.
327 Figure 7(a) shows that the fine dust concentration is generally poor, while Figure 7(b) shows that the
328 fine dust concentration is generally good. Similar concentrations can be found by comparing the
329 measured concentrations of AQMS.
330   Although the fine dust patterns constructed through modeling are similar to the AQMS values,
331 they differ when examining only the cells in which AQMS units are installed. This issue will be
332 addressed in section 4.

333 *3.2 Comparison and Analysis of Existing Methodology*

334 3.2.1 Comparison and Analysis of Fine Dust Concentration Maps

335   The fine dust information that is provided to citizens is received from the AQMS closest to the
336 query location. This existing methodology was employed to generate concentration maps using GIS
337 Euclidean distance measurements. The maps for the four investigated areas were constructed by
338 Euclidean distance measurement with the four AQMS devices in the target sites as starting points.
339   The concentration maps created through particulate matter dispersion modeling according to
340 the method developed in this study were generated based on the fine dust concentrations of over
341 16,000 cells, where each concentration was calculated within a 50 m × 50 m cell of the target site.
342   Figure 8 presents sample PM2.5 concentration maps created using the existing methodology and
343 PM2.5 dispersion modeling. In Map 1, 2, and 3 of Figure 8, differences can be seen between the maps
344 generated using the two techniques. According to the existing methodology, the PM2.5
345 concentrations are "Good" or "Moderate," while those obtained via dispersion modeling are
346 frequently "Unhealthy" or "Very Unhealthy." These differences could mean that the PM2.5
347 concentration information provided to citizens is inaccurate. In map 4 of Figure 8, the results of the
348 existing methodology and PM2.5 dispersion modeling are similar. While some of the modeling values
349 are designated as "Unhealthy," they comprise a relatively insignificant portion of the overall map.

Figure 7. Comparison of PM2.5 concentration maps constructed using the existing methodology and PM2.5 dispersion modeling.

Table 2 provides a comparison of the results obtained using the existing methodology and PM2.5
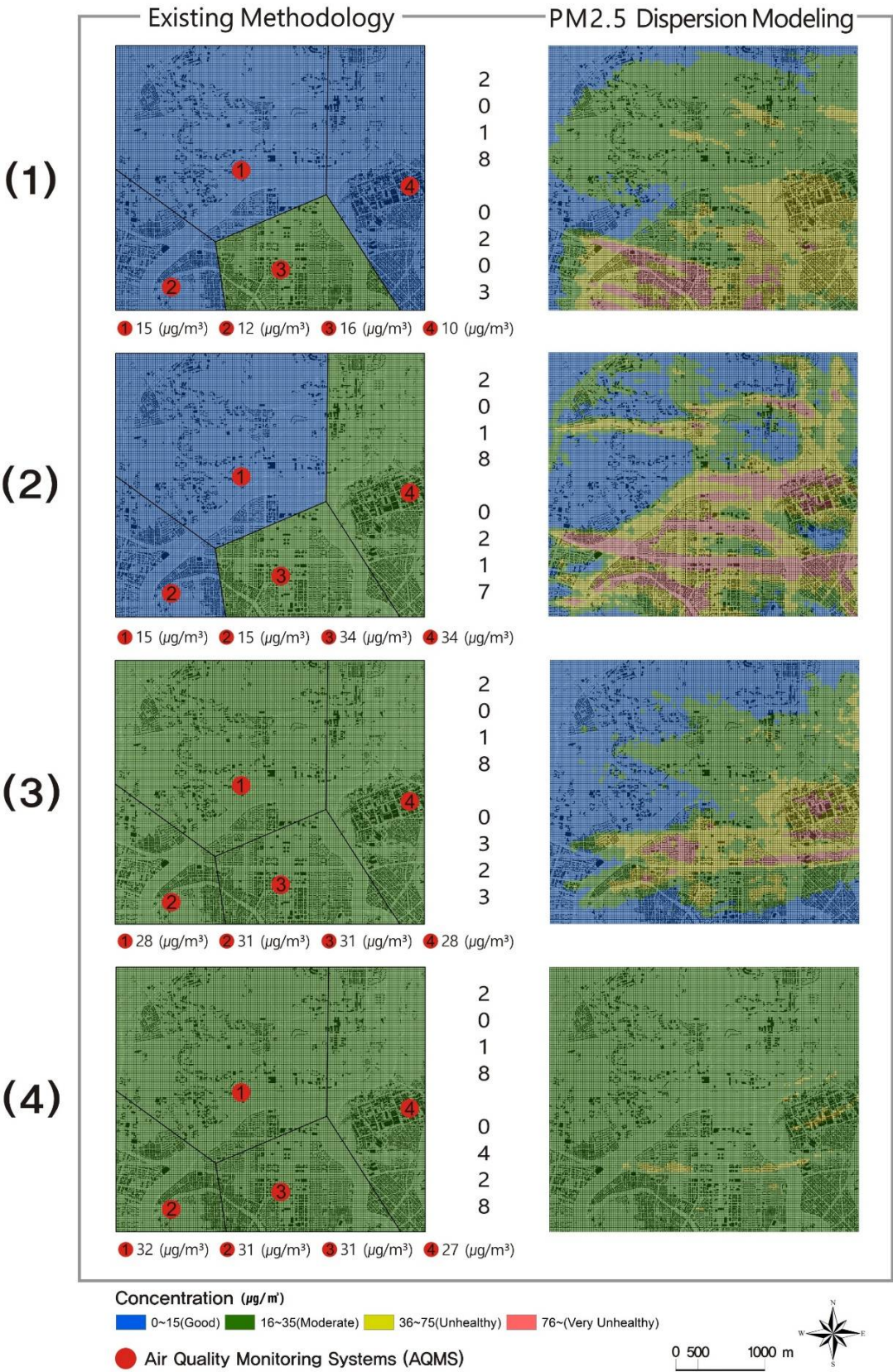
354   dispersion modeling as ratios.

355   **Table 2.** Comparison of concentration ratios according to the existing methodology and PM2.5 dispersion
356   modeling.

Concentration ($\mu g/m^3$)	Existing Methodology (%)				PM2.5 Dispersion Modeling (%)			
	(1) 20180203	(2) 20180217	(3) 20180323	(4) 20180428	(1) 20180203	(2) 20180217	(3) 20180323	(4) 20180428
Good (0–15)	82.72024	56.30357	0	0	16.25	31.35714	46.66667	0
Moderate (16–35)	17.27976	43.69643	100	100	52.19048	25.85714	33.20238	98.27976
Unhealthy (36–75)	0	0	0	0	26.06548	27.76786	16.64286	1.720238
Very Unhealthy (>76)	0	0	0	0	5.494048	15.01786	3.488095	0

357
358   In case 1 of Table 2, the differences between the concentrations obtained using the existing
359   methodology and PM2.5 dispersion modeling can be seen quantitatively in Table 2. According to the
360   existing methodology, the concentration is "Good," meaning that most people can engage in outdoor
361   activities safely in more than 80% of the area. However, according to the modeling results, more than
362   30% of the concentrations are bad, and "Moderate" concentrations exist in more than 50% of the areas.
363   The fine dust standards of WHO and developed nations state that "Moderate" concentrations can
364   have adverse effects on vulnerable populations, such as children and the elderly. Aside from case 4
365   of Table 2, there are significant differences between the values obtained using the two methodologies
366   according to Table 2.
367   Figure 9 presents PM10 concentration maps created using the existing methodology and
368   particulate matter dispersion modeling. Map 1 of Figure 9 exhibits "Moderate" fine dust
369   concentrations everywhere, but the modeling results display "Good," "Moderate," "Unhealthy," and
370   "Very Unhealthy" concentrations. Map 2 of Figure 9 only shows the areas near AQMS-3 as being
371   "Unhealthy" and the other areas as "Moderate," while the modeling results show "Good,"
372   "Moderate," "Unhealthy," and "Very Unhealthy" concentrations. Map 3 of Figure 9 differs from the
373   others. According to the existing methodology, the areas near AQMS-1 have "Unhealthy"
374   concentrations, but the modeling results show "Good" or "Moderate" concentrations. Finally, map 4
375   of Figure 9 indicates that the fine dust concentration is generally "Moderate," but also exhibits
376   extensive regions with "Very Unhealthy" concentrations.
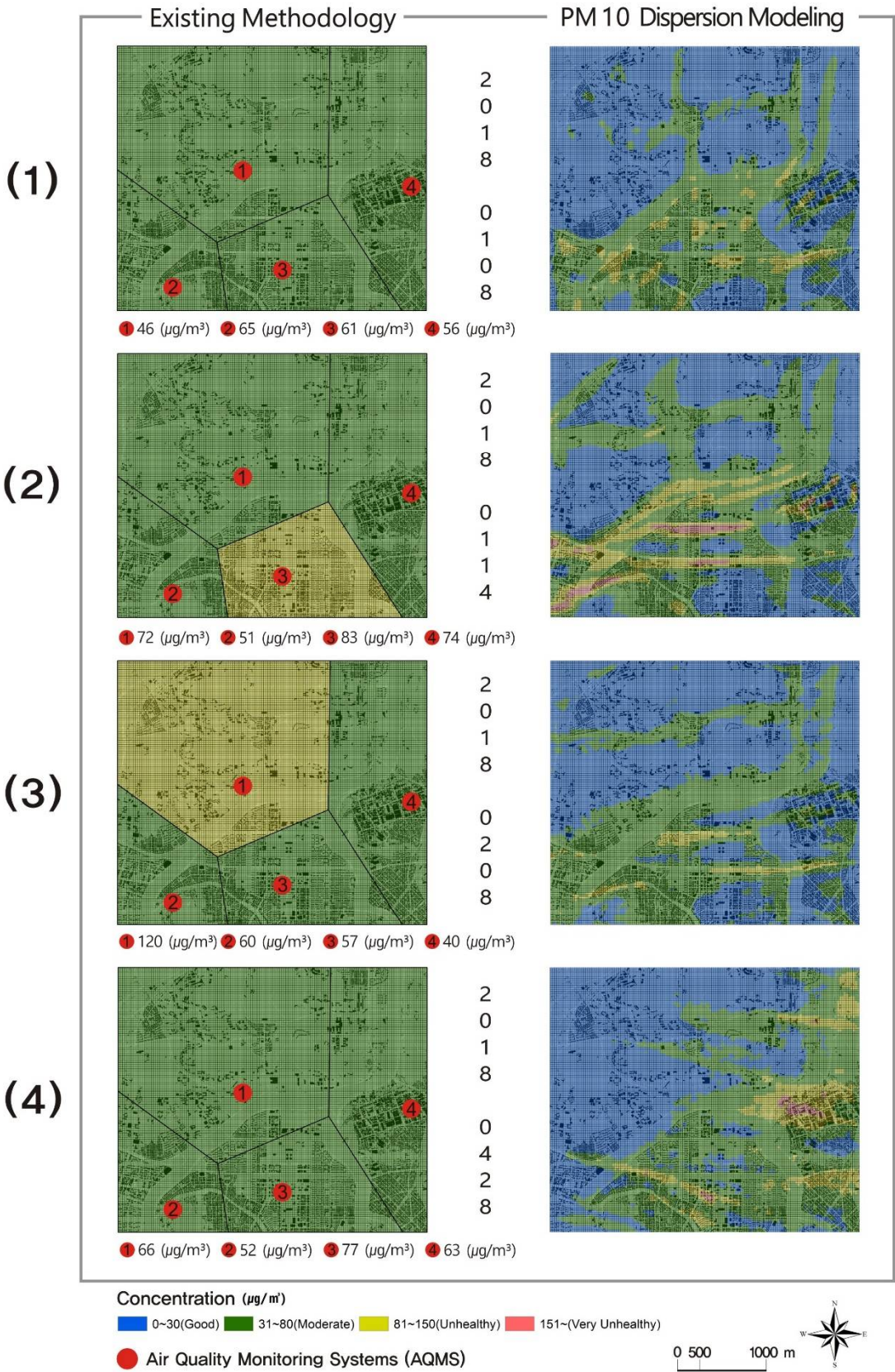
Figure 8. Comparison of PM10 concentration maps constructed using the existing methodology and PM10 dispersion modeling.

Table 3 provides a comparison of the concentration results obtained using the existing methodology and PM10 dispersion modeling as ratios.

382   **Table 3.** Comparison of concentration ratios obtained using the existing methodology and PM10 dispersion
383   modeling.

Concentration (μg/m³)	Existing Methodology (%)				PM10 dispersion modeling (%)			
	(1) 20180108	(2) 20180114	(3) 20180208	(4) 20180428	(1) 20180108	(2) 20180114	(3) 20180208	(4) 20180428
Good (0–30)	0	0	0	0	58.67857	47.38095	54.54762	48.66071
Moderate (31–80)	100	82.72024	56.89881	100	36.65476	40.64286	43.09524	41.875
Unhealthy (81–150)	0	17.27976	43.10119	0	4.642857	10.08929	2.357143	8.77381
Very Unhealthy (>151)	0	0	0	0	0.02381	1.886905	0	0.690476

384   In case 1 of Table 3, all of the concentrations are "Moderate," according to the existing
385   methodology, but the modeling results show all of the concentration levels. The results for case 2
386   indicate that approximately 2% of the sections have "Very Unhealthy" concentrations, but these
387   regions constitute an area of roughly 800,000 m², the majority of which is residential. The spatial
388   interpretation will be addressed in greater detail in section 4. In case 3 of Table 3, the "Unhealthy"
389   areas comprise approximately 43% according to the existing methodology, indicating restrictions on
390   outdoor activities and ventilation, but these areas constitute only about 2% in the modeling results.
391   In case 4 of Table 3, the overall target site is at a "Moderate" level according to the existing
392   methodology, but the modeling results show PM10 concentrations at "Unhealthy" and "Very
393   Unhealthy" levels in approximately 10% of the target site. Thus, an area of approximately 4,000,000
394   m², which was concentrated around residential areas, had high PM10 concentrations.

395   3.2.2 Comparison and Analysis of Population Exposed to Fine Dust

396   The populations exposed to PM2.5 according to the existing methodology and PM2.5 dispersion
397   modeling were also compared. Figure 10 depicts the areas where people live on the PM2.5
398   concentration maps constructed using the existing methodology and PM2.5 dispersion modeling. In
399   map 1, all of the people are exposed to "Moderate" concentrations, according to the existing
400   methodology, but based on the modeling results, approximately 100,000 people are exposed to
401   "Unhealthy" and "Very Unhealthy" concentrations. In map 2, approximately 100,000 people are
402   exposed to "Good" concentrations, according to the existing methodology, but the modeling results
403   show that over 170,000 people are exposed to "Unhealthy" and "Very Unhealthy" levels.
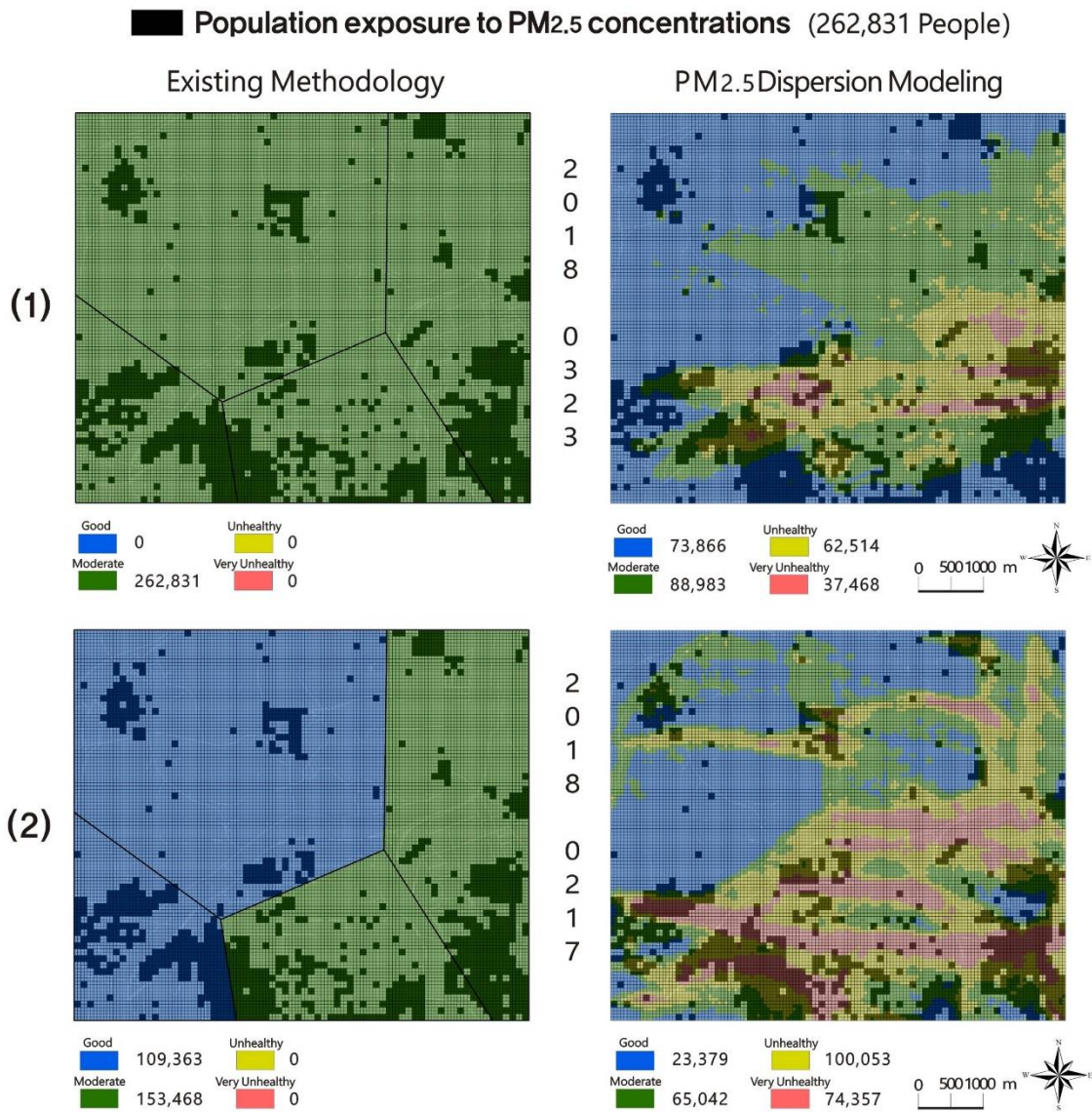
Figure 9. Comparison of populations exposed to different PM2.5 concentrations, according to the existing methodology and PM2.5 dispersion modeling.

Similarly, the populations exposed to PM10 according to the existing methodology and dispersion modeling were compared. Figure 11 depicts the areas where people live on the PM10 concentration maps constructed using the existing methodology and dispersion modeling. In map 1, no one is exposed to "Good" or "Very Unhealthy" concentrations, according to the existing methodology, but the modeling results show that more than 70,000 people are exposed to "Good" levels and more than 10,000 are exposed to "Very Unhealthy" levels. In map 2, all of the population is exposed to "Moderate" concentrations, according to the existing methodology, but the modeling results show that the population is exposed to all concentration levels.
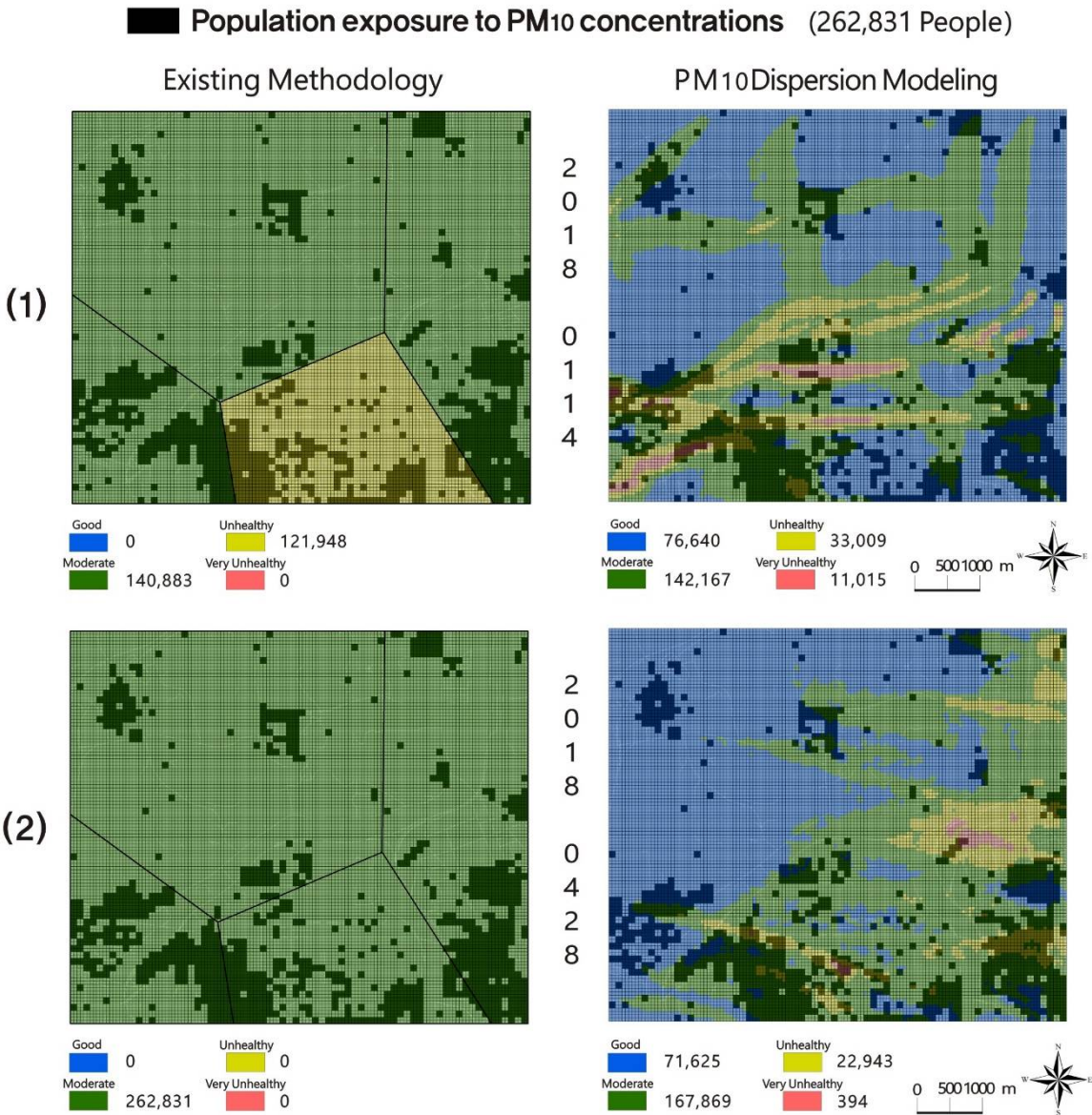
Figure 101. Comparison of populations exposed to various PM10 concentrations, according to the existing methodology and PM10 dispersion modeling.

4. Discussion

4.1 Particulate Matter Dispersion Modeling

In the particulate matter dispersion model developed in the present study, the meteorological and Lagrangian particle dispersion models are utilized to determine the dispersion of fine dust in urban areas. Differences were observed between the fine dust concentration maps created using this model and those currently provided to citizens. As mentioned above, fine dust information is acquired from the nearest AQMS. However, [13] stated that the distribution of atmospheric pollutants must be predicted by taking into account numerous variables, including land use, pollution source location, traffic volume, and temperature. Thus, the particulate matter dispersion model that considers these variables is more precise than the existing methodology.

There are various techniques for fine dust distribution prediction, but that currently used to provide information to citizens is a very simple one based on Euclidean distance measurement. In

430 this method, spaces are simply divided according to the distances measured between AQMS units,
431 without regard to any other variables. The fine dust maps obtained using the existing methodology
432 in Figures 8 and 9 depict the fine dust concentrations in four areas, and each can only be verified with
433 identical numerical values. In addition, Tables 2 and 3 show that, according to the existing
434 methodology, there are almost no "Unhealthy" and "Very Unhealthy" concentrations, which differs
435 from the results obtained by modeling. The kriging method [15] is more precise than the existing
436 methodology (Euclidean distance measurement), and can be used to forecast the air quality of an
437 entire target site. Although this methodology has higher predictive accuracy with a higher number
438 of real measurement values, some AQMS devices were installed in the target sites in this study, and
439 thus, fine dust measurements could have been inaccurate if the above method had been employed.
440 Kriging and IDW are spatial statistics methods based on GIS, but these methods would not have been
441 able to reflect the characteristics of the target sites in this study, such as land use or emission source.

442   Recently, high-dimensional data analysis methodologies have also been employed. 17] utilized
443 meteorological and pollutant data obtained over the previous 6 years and forecasted future fine dust
444 concentrations via machine learning methods. This methodology differs from that employed in the
445 present study as it involves the use of numerous data points observed in the past to forecast the future.
446 The methodology utilized in this study enables current concentrations or those 1 h later to be
447 determined using meteorological data that is provided in 1 h intervals. Unlike in the study conducted
448 by [18], it was possible to extract accurate fine dust concentrations through modeling that minutely
449 reflected the characteristics of the investigated areas in the present study. Future research that merges
450 the modeling employed in this study with machine learning or AI methods to deduce fine dust
451 concentrations could be meaningful.

452   The Lagrangian particle dispersion model used in the particulate matter dispersion model that
453 was developed in this study is a 3D numerical analysis model that is primarily utilized with the
454 Eulerian model when modeling atmospheric dispersion. However, it has the disadvantage that its
455 results are difficult to compare with measurements from air pollution monitoring stations. In
456 addition, the modeling results shown in Figures 6 and 7 indicate that there are differences between
457 the AQMS fine dust concentrations and modeling values in identical cells. The reason for this
458 discrepancy appears to be the complexity of the algorithm that includes the dispersion and movement
459 of fine dust based on wind direction and speed, as well as land use and emission source.

460 *4.2 Spatial Distribution of Fine Dust and Exposed Populations*

461   The results of the particulate matter dispersion model developed in this study revealed high fine
462 dust concentrations mainly in the southern and eastern areas, where a river was flowing horizontally
463 through the center of the region. The target site had a mountainous area to the north whose parts
464 remained mostly urbanized. The complex terrain was reflected in the developed particulate matter
465 dispersion model to calculate the meteorological field. As such, even if the fine dust concentration
466 was high in the south, the effects of wind blowing in the mountainous areas in the north resulted in
467 low fine dust concentrations. AQMS-1, which is located in the north, also yielded mostly lower
468 concentrations than the AQMS located in the remaining three areas.

469   According to existing research methodologies, the AQMS data at one location represent the
470 entirety of the corresponding area, while the modeling results provide fine dust concentrations by
471 cell. The modeling results in Figure 8 reveal high PM2.5 concentrations in the south and east where
472 there is a high density of buildings. The reason for this finding can be approached from a variety of
473 perspectives. First, industrial complexes, which are the leading source of pollution, are located in the
474 east, where there is also a developed road network with a significant volume of traffic. Studies in
475 which fine dust concentrations due to vehicles have been measured on the sides of roads based on
476 elevation [40, 41] have indicated that high fine dust concentrations occur at low elevations due to
477 vehicles. It is also necessary to consider high fine dust concentration values that occur due to
478 buildings. High-rise apartments and other buildings are located in areas with high concentrations,
479 and 3D building and structural information was also utilized in the developed particulate matter
480 dispersion model. Although they did not address buildings, [42] performed fine dust concentration

481 measurements by elevation along roads lined with tall trees on both sides. Their results indicated that
482 there were higher fine dust concentrations than in the surrounding areas. It is possible that high
483 buildings impact wind paths similarly, causing fine dust to stagnate between buildings.
484   In addition to spatial fine dust concentration analysis, it is also necessary to analyze exposed
485 populations, which is important for urban and environmental planning. A small portion of the
486 population may be exposed in areas where poor fine dust concentrations are widely distributed, and
487 a large portion of the people in densely populated areas may be exposed even if poor fine dust
488 concentrations are narrowly distributed. For instance, the PM2.5 concentrations on February 17, 2018,
489 in Figures 8 and 10 show that while approximately 40% of the target area had poor PM2.5 levels,
490 around 70% of the entire population was exposed to those levels. Similarly, the PM10 concentrations
491 on January 14, 2018, in Figures 9 and 11 reveal that while only 10% of the target area had poor PM10
492 concentrations, over 40,000 people were exposed to those concentrations.
493   To achieve cities that are free from fine dust, the creation of sustainable cities and environmental
494 planning based on the above results that account for land use and exposed populations is necessary,
495 as well as the use of green spaces and proper wind paths and continuous environmental monitoring
496 of emission sources.

5. Conclusions

498   The present study was conducted with an awareness of the errors in the fine dust concentrations
499 currently provided to citizens. Motivated by this awareness, the fine dust concentrations obtained
500 using the existing methodology and dispersion modeling were compared with each other and
501 analyzed. The exposed populations according to these two methodologies were also examined. While
502 the fine dust concentrations currently available are simply representative values provided by AQMS,
503 those obtained by modeling account for the present conditions of the target site and meteorological
504 factors. Thus, the results yielded by the two methodologies differed from each other. Modeling was
505 able to provide the detailed spatial distributions of fine dust concentrations and exposed populations.
506 As the harm caused by fine dust is becoming more severe worldwide, this research will contribute to
507 sustainable urban and environmental planning.
508   Since the emission information used in the particulate matter dispersion model developed in
509 this study was survey data rather than real-time observations, future studies should be conducted
510 using real-time observations. In addition, when exposed populations are calculated in future studies,
511 smartphone data should be employed, and the exposed population should be calculated by taking
512 into account current location rather than place of residence.
513   Above all, to provide fine dust concentrations, such as those deduced in this study, through
514 smartphones or websites in real time, research and technical skills related to data connections,
515 algorithm loading, and communications are needed from an information systems perspective, and
516 systems and policies that can contribute to sustainable urban environments should be considered.

Author Contributions: The first author, Seungwoo Son, developed the flow of this study, wrote most of manuscript, and performed the dispersion modeling. Hyungjin Jeon, Dongwoo Kim, and Jaejin Yu wrote some of the manuscript and conducted a GIS analysis. Seogcheol Kim and Kyunghak Cho performed the particle matter dispersion modeling. Youngeun Kang reviewed the manuscript and contributed to the research design.

Acknowledgments: This study was funded by the Korea Environmental Industry & Technology Institute (KEITI) under grant [number: 2016000200009] and conducted by the Korea Environment Institute (KEI).

Conflicts of Interest: The authors declare no conflict of interest.

References

1.   World Health Organization. *Ambient Air pollution: A Global Assessment of Exposure and Burden of Disease.* World Health Organization, Geneva, Switzerland, 2016, ISBN: 9789241511353.

2.   Guerreiro, C.B.; Foltescu, V.; De Leeuw, F. Air quality status and trends in Europe. *Atmos. Environ.* **2014**, *98*, 376-384.

3.   Schneider, P.; Castell, N.; Vogt, M.; Dauge, F.R.; Lahoz, W.A.; Bartonova, A. Mapping urban air quality in near real-time using observations from low-cost sensors and model information. *Environ. Int.* **2017**, *106*, 234-247.

4.   Li, N.; Han, W.; Tang, J.; Bian, J.; Sun, S.; Song, T. Pollution characteristics and human health risks of elements in road dust in Changchun, China. *Int. J. Environ. Res. Public Health.* **2018,** *15*(9), 1843.

5.   Iizuka, A.; Shirato, S.; Mizukoshi, A.; Noguchi, M.; Yamasaki, A.; Yanagisawa, Y. A cluster analysis of constant ambient air monitoring data from the Kanto region of Japan. *Int. J. Environ. Res. Public Health.* **2014,** *11*(7), 6844-6855.

6.   Kim, P. Operating an environmentally sustainable city using fine dust level big data measured at individual elementary schools. *Sustainable Cities and Society.* **2018,** *37*, 1-6.

7.   Numan, M.S.; Brown, J.P.; Michou, L. Impact of air pollutants on oxidative stress in common autophagy-mediated aging diseases. *Int. J. Environ. Res. Public Health.* **2015,** *12*(2), 2289-2305.

8.   Nafissa, B.; Bouzerna, N.; Chettibi, H. Assessment of the petrochemical industry pollution on the Skikda bay, Algeria. *Int. J. Environ. Res. Public Health.* **2005,** *2*(3), 463-468.

9.   Wang, J.; Niu, T.; Wang, R. Research and application of an air quality early warning system based on a modified least squares support vector machine and a cloud model. *Int. J. Environ. Res. Public Health.* **2017,** *14*(3), 249.

10.   Pope III, C.A.; Dockery, D.W. Health effects of fine particulate air pollution: lines that connect. *J. Air Waste Manag. Assoc.* **2006**, *56*(6), 709-742.

11.   Yanosky, J.D.; Paciorek, C.J.; Laden, F.; Hart, J.E.; Puett, R.C.; Liao, D.; Suh, H.H. Spatio-temporal modeling of particulate air pollution in the conterminous United States using geographic and meteorological predictors. *Environ. Health* **2014**, *13*(1), 63.

12.   Beelen, R.; Hoek, G.; Pebesma, E.; Vienneau, D.; de Hoogh, K.; Briggs, D.J. Mapping of background air pollution at a fine spatial scale across the European Union. *Sci. Total Environ.* **2009**, *407*(6), 1852-1867.

13.   Rodríguez, M.C.; Dupont-Courtade, L.; Oueslati, W. Air pollution and urban structure linkages: Evidence from European cities. *Renew. Sustain. Energ. Rev.* **2016**, *53*, 1-9.

14.   Liu, Z.; Xie, M.; Tian, K.; Gao, P. GIS-based analysis of population exposure to PM2. 5 air pollution—A case study of Beijing. *J. Environ. Sci.* **2017**, *59*, 48-53.

15.   Zheng, Y.; Liu, F.; Hsieh, H.P. U-Air: When urban air quality inference meets big data. In Proceedings of the 19th ACM SIGKDD International Conference on Knowledge Discovery and Data Mining. ACM: Chicago, IL, 2013, pp. 1436-1444.

16.   Deville Cavellin, L.; Weichenthal, S.; Tack, R.; Ragettli, M.S.; Smargiassi, A.; Hatzopoulou, M. Investigating the use of portable air pollution sensors to capture the spatial variability of traffic-related air pollution. *Environ. Sci. Technol.* **2015**, *50*(1), 313-320.

17.   Kleine Deters, J.; Zalakeviciute, R.; Gonzalez, M.; Rybarczyk, Y. Modeling PM2.5 urban pollution using machine learning and selected meteorological parameters. *J. Electr. Comput. Eng.* **2017**, *2017*, 5106045.

18.   Alegana, V.A.; Atkinson, P.M.; Pezzulo, C.; Sorichetta, A.; Weiss, D.; Bird, T.; Erbach-Schoenberg, E.; Tatem, A.J. Fine resolution mapping of population age-structures for health and development applications. *J. Royal Soc. Interface* **2015**, *12*(105), 20150073.

19.   Stevens, F.R.; Gaughan, A.E.; Linard, C.; Tatem, A.J. Disaggregating census data for population mapping using random forests with remotely-sensed and ancillary data. *PloS One* **2015**, *10*(2), e0107042.

20.   Kim, S.C.; Lee, J.S.; Yun, J.I.; Kang, J.H.; Kim, W.S. Study on Lagrangian heat source tracking method for urban thermal environment simulations. *J. Korean Soc. Atmos. Environ.* **2017**, *33*(6), 583-592.

21.   Panofsky, H.A.; Dutton, J.A. *Atmospheric Turbulence: Models and Methods for Engineering Applications*, Wiley: New York, NY, USA, 1984, p. 397, ISBN: 9780471057147.

22.   Van Ulden, A.P.; Holtslag, A.A.M. Estimation of atmospheric boundary layer parameters for diffusion applications. *J. Clim. Appl. Meteorol.* **1985**, *24*(11), 1196-1207.

23.   De Bruin, H.A.R.; Holtslag, A.A.M. A simple parameterization of the surface fluxes of sensible and latent heat during daytime compared with the Penman-Monteith concept. *J. Appl. Meteorol.* **1982**, *21*(11), 1610-1621.

24.   Macdonald, R.W.; Griffiths, R.F.; Hall, D.J. An improved method for the estimation of surface roughness of obstacle arrays. *Atmos. Environ.* **1998**, *32*(11), 1857-1864.

25. Macdonald, R. W. Modelling the mean velocity profile in the urban canopy layer. *Boundary Layer Meteorol.* **2000**, *97*(1), 25-45.

26. Bentham, T.; Britter, R. Spatially averaged flow within obstacle arrays. *Atmos. Environ.* **2003**, *37*(15), 2037-2043.

27. Hanna, S.R.; Britter, R.E. *Wind Flow and Vapor Cloud Dispersion at Industrial and Urban Sites*, John Wiley & Sons: Hoboken, NJ, USA, 2010; Volume 7, ISBN: 9780816908639.

28. Liu, M.K.; Yocke, M.A. Siting of wind turbine generators in complex terrain. *J. Energ.* **1980**, *4*(1), 10-16.

29. Mahrt, L. Momentum balance of gravity flows. *J. Atmos. Sci.* **1982**, *39*(12), 2701-2711.

30. Allwine, K.J.; Whiteman, C.D. *MELSAR: A Mesoscale Air Quality Model for Complex Terrain. Overview, Technical Description and User's Guide (No. PNL-5460-Vol. 1)*. Pacific Northwest Labs, Richland, WA, USA, 1985; Volume 1.

31. Stohl, A.; Klimont, Z.; Eckhardt, S.; Kupiainen, K.; Shevchenko, V.P.; Kopeikin, V.M.; Novigatsky, A.N. Black carbon in the Arctic: the underestimated role of gas flaring and residential combustion emissions. *Atmos. Chem. Phys.* **2013**, *13*(17), 8833-8855.

32. Lin, J.C.; Gerbig, C.; Wofsy, S.C.; Andrews, A.E.; Daube, B.C.; Davis, K.J.; Grainger, C.A. A near-field tool for simulating the upstream influence of atmospheric observations: The stochastic time-inverted Lagrangian transport (STILT) model. *J. Geophys. Res. Atmos.* **2003**, *108*(D16).

33. Witham, C.S.; Hort, M.C.; Potts, R.; Servranckx, R.; Husson, P.; Bonnardot, F. Comparison of VAAC atmospheric dispersion models using the 1 November 2004 Grimsvötn eruption. *Meteorol. Appl.* **2007**, *14*(1), 27-38.

34. Stein, A.F.; Draxler, R.R.; Rolph, G.D.; Stunder, B.J.; Cohen, M.D.; Ngan, F. NOAA's HYSPLIT atmospheric transport and dispersion modeling system. *Bull. Am. Meteorol. Soc.* **2015**, *96*(12), 2059-2077.

35. Eckhardt, S.; Cassiani, M.; Evangeliou, N.; Sollum, E.; Pisso, I.; Stohl, A. Source–receptor matrix calculation for deposited mass with the Lagrangian particle dispersion model FLEXPART v10. 2 in backward mode. *Geosci. Model Dev.*, **2017**, *10*, 4605-4618.

36. Borgas, M.S.; Sawford, B.L. A family of stochastic models for two-particle dispersion in isotropic homogeneous stationary turbulence. *J. Fluid Mech.* **1994**, *279*, 69-99.

37. Raupach, M.R.; Legg, B.J. Turbulent dispersion from an elevated line source: measurements of wind-concentration moments and budgets. *J. Fluid Mech.* **1983**, *136*, 111-137.

38. Talen, E. Neighborhoods as service providers: a methodology for evaluating pedestrian access. *Environ. Plan. B* **2003**, *30*(2), 181-200.

39. Son, S.W.; Ahn, T.M. Sensitivity analysis on the population within and outside of the Urban Park Service areas - Focused on Daegu Metropolitan City neighborhood parks and resident registration number data. *J. Korean Inst. Landscape Archit*. **2013**, *41*(5), 9-18.

40. Weber, K.; Heweling, G.; Fischer, C.; Lange, M. The use of an octocopter UAV for the determination of air pollutants–a case study of the traffic induced pollution plume around a river bridge in Duesseldorf, Germany. *Int. J. Environ. Sci.* **2017**, *2*, 63-68.

41. Villa, T.F.; Jayaratne, E.R.; Gonzalez, L.F.; Morawska, L. Determination of the vertical profile of particle number concentration adjacent to a motorway using an unmanned aerial vehicle. *Environ. Pollut.* **2017**, *230*, 134-142.

42. Liu, F.; Zheng, X.; Qian, H. Comparison of particle concentration vertical profiles between downtown and urban forest park in Nanjing (China). *Atmos. Pollut. Res*. **2018**, *9*(5), 829-839.